International Journal of Nanomedicine

Dovepress
open access to scientific and medical research

Open Access Full Text Article

ORIGINAL RESEARCH

A Smart CA IX-Targeting and pH-Responsive Nano-Mixed Micelles for Delivery of FB15 with Superior Anti-Breast Cancer Efficacy

XingYun Liu[1,*], JingDuo Zhao[2,*], FuRong Liu[1], ZhiZhong Xie[2], XiaoYong Lei[2], Zhe Wang[3], Zerui Yang[4], YuSheng Zhou[1,3], GuoTao Tang[2]

[1]The Affiliated Nanhua Hospital, Department of Pharmacy, Hengyang Medical School, University of South China, Hengyang, 421001, People's Republic of China; [2]Institute of Pharmacy and Pharmacology, Hunan Province Cooperative Innovation Center for Molecular Target New Drug Study, University of South China, Hengyang, 421001, People's Republic of China; [3]The Second Affiliated Hospital, Department of Pharmacy, Hengyang Medical School, University of South China, Hengyang, 421001, People's Republic of China; [4]NMPA Key Laboratory for Technology Research and Evaluation of Pharmacovigilance, Guangdong Pharmaceutical University, Guangzhou, 510086, People's Republic of China

*These authors contributed equally to this work

Correspondence: YuSheng Zhou, The Affiliated Nanhua Hospital, Hengyang Medical School, University of South China, Hengyang, 421001, People's Republic of China, Email yszhou08@126.com; GuoTao Tang, Institute of Pharmacy and Pharmacology, Hunan Provincial Key Laboratory of Tumor Microenvironment Responsive Drug Research, Hengyang Medical School, Hengyang, Hunan, 421001, People's Republic of China, Email tgtzq@163.com

Background: Breast cancer treatment has been a global puzzle, and targeted strategies based on the hypoxic tumor microenvironment (TME) have attracted extensive attention. As a signature transcription factor overexpressed in hypoxia tumor, hypoxia-inducible factor-1 (HIF-1) contribute to cancer progression. Compound 7-(3-(2-chloro-1H-benzo[d]1midazole-1-yl) propoxy)-2-(3,4,5-trimethoxyphenyl)-4H-chromen-4-one, synthesized and named FB15 in our earlier research, a potential inhibitor of HIF-1α signaling pathway, has been proved a promising drug candidate for many kinds of cancer chemotherapy. However, the poor solubility and undesirable pharmacokinetics of FB15 leads to limited treatment efficacy of tumor, which ultimately restricts its potential clinical applications. Carbonic anhydrase IX (CAIX), a tumor cell transmembrane protein, was overexpressed in hypoxia tumor site. Acetazolamide (AZA), a highly selective ligand targeting CAIX, can be utilized to delivery FB15 to hypoxia tumor site.

Methods: In this study, we prepared and characterized FB15 loaded nano-mixed micelles with the AZA conjugated poloxamer 188 (AZA-P188) and D-a-Tocopherol Polyethylene 1000 Glycol Succinate (TPGS), denoted as, AZA-P188/TPGS@FB15. Its delivery efficiency in vitro and in vivo was assessed by in vitro drug release, cytotoxicity assay, cellular uptake, and in vivo pharmacokinetics and fluorescence imaging. Finally, therapeutic effect of AZA-P188/TPGS@FB15 was investigated using a preclinical breast cancer subcutaneous graft model in vivo.

Results: In vitro studies revealed that AZA-P188/TPGS@FB15 could efficiently target breast cancer cells mediated by CAIX receptor, trigger FB15 release in response to acidic condition, and enhance cellular uptake and cytotoxicity against breast cancer cells. The pharmacokinetic studies showed that FB15-loaded AZA-functionalized micelles exhibited significantly increased AUC_{0-t} over free FB15. In vivo imaging demonstrated that AZA-functionalized micelles significantly increased the drug distribution in the tumor site. In vivo experiments confirmed that AZA-P188/TPGS@FB15 exhibited superior inhibition of tumor growth in nude mice with good biosafety.

Conclusion: AZA-P188/TPGS@FB15 hold promise as a potentially effective therapeutic way for breast cancer. Its targeted delivery system utilizing AZA as a carrier shows potential for improving the efficacy of FB15 in cancer therapy.

Keywords: carbonic anhydrase IX-targeting, FB15, hypoxia inducible factor-1, nano-mixed micelles, pH-responsive

Introduction

Breast cancer (BC) prevails as a major burden on global healthcare, being the most common cancer incidence among women.[1] Compared to normal breast tissue, breast cancer exhibits significantly lower oxygen partial pressure as a type of solid tumors,[2]

Received: 26 April 2024
Accepted: 16 September 2024
Published: 9 October 2024

because the oxygen consumption of rapidly proliferating tumor cells exceeds the oxygen supply of tumor vasculature. Hypoxia accelerates malignancy progression and metastasis by causing angiogenesis and the over-expression of certain protein products essential for tumor growth.[3,4] Reduced oxygen availability triggers the activation of hypoxia-inducible factors-1 (HIF-1), a heterodimeric protein made up of the HIF-1α and HIF-1β subunits. As an oxygen-dependent transcriptional regulator, HIF-1 upregulates glycolysis by increasing the glucose uptake and the expression of glycolytic enzymes, such as lactate dehydrogenase A (LDHA), pyruvate dehydrogenase kinase-1 (PDK1) and hexokinase II (HK II), by raising the expression of glucose transporter protein-1 (GLUT1) which plays a direct role in glucose metabolism via glycolysis.[5] The levels of HIF-1α protein dramatically increase in hypoxic cancer cells.[6] Clinical evidence supports that high-level expression of HIF-1α protein in diagnostic tumor biopsies from multiple kinds of breast cancers was positively associated with increased risk of poor outcome in unselected breast cancer patients,[7,8] as well as its contributions to malignant behavior and therapeutic resistance contributions.[9] Notably, the application of HIF-1α inhibitor, whether directly or indirectly decreasing the levels of HIF-1α, in combination with other anti-cancer agents, has exhibited significant improvements in radiotherapy and chemotherapy, reversing tumor drug resistance, and reducing tumor cell metastasis.[10–13] As a pivotal regulator in hypoxic tumor cells, HIF-1α presents a prospective target for the creation of innovative antitumor medications against solid tumors like breast cancer.[10] In recent decades, several targeting inhibitors HIF-1α have been identified (Apigenin,[11] YC-1[10], Honokiol,[12] Acriflavine[13]). Furthermore, it has been demonstrated that some approved drugs (Panzem®, Velcade®) directly or indirectly inhibit of HIF-1α.[14,15] Nevertheless, no selective HIF-1α inhibitor has been clinically approved by Food and Drug Administration (FDA) for cancer treatment. Therefore, the development of effective anticancer drugs that specifically target HIF-1α is urgently needed.

FB15 (7-(3-(2-chloro-1H-benzo[d]midazole-1-yl)propoxy)-2-(3,4,5-trime-thoxyphenyl)-4H-chromen-4-one), a recently synthesized flavonoid-benzimidazole derivative, was designed to target HIF-1α signaling pathway, as demonstrated in our earlier research.[16] In vitro experiments have shown that FB15-induced apoptosis in tumor cells and exhibits strong antiproliferation activity against the mouse fore-stomach carcinoma (MFC) cell lines[16] and human gastric cancer MGC-803 cell lines but minimal cytotoxicity towards normal stomach cells.[17] Moreover, FB15 has demonstrated significant antitumor activity against the transplanted tumors growth in mice, surpassing that of the clinical anticancer medicine 5-Fluorouracil (5-Fu).[17] Notably, FB15 has been found to significantly inhibit the HIF-1α signaling pathway, such as the activity and expression of HIF-1α and glycolytic enzymes HK-II, PFKP at the transcriptional level.[17] Taken together, its great anti-tumor activity, low toxicity profile and novel target make FB15 an especially promising candidate for cancer chemotherapy and metastasis treatment.[16,17] However, its poor solubility, suboptimal bioavailability and limited tumor permeability ultimately hamper its potential clinical applications. A smart nano-delivery system integrated with dual-functionalities of active targeted delivery and responsive drug release can enhance therapeutic efficacy of FB15 and mitigate its side effects, thus lighting up the hope for the effective treatment of malignancies with FB15 in clinical.

The unique hypoxic microenvironment of tumors provides conditions for this "smart" targeting-responsive drug delivery. Hundreds of genes, like the carbonic anhydrase IX (CAIX) regulated by HIF-1α, were over-expressed in the hypoxic microenvironment. CAIX is a tumor-associated transmembrane-binding enzyme for regulating intra-tumoral pH, which facilitated to tumor proliferation[18,19] Significantly increased CAIX expression has been demonstrated in many types of malignant tumors including breast cancer, which is a marker of poor prognosis.[20–22] In addition, acidic pH is also a common characteristic of solid tumors. Recently, CAIX has been unveiled to affect cellular metabolism. Inhibition of CAIX activity significantly mediates cellular acidification,[23] which contributes to accelerating drug release for pH-sensitive delivery systems. Hence, CAIX has attracted much attention as an appealing epitope for tumor-specific therapy.[24] Nanomedicines anchored with CAIX inhibitors could accomplish active tumor-targeting delivery to the hypoxic location as well as more effective intra-tumoral enrichment through a specific ligand-receptor interaction.[25,26]

Taken this into consideration, we designed and synthesized smart nano-mixed micelles consisting of Acetazolamide (AZA) conjugated poloxamer 188 (AZA-P188) and α-tocopherol-polyethylene glycol-succinic acid (TPGS), named AZA-P188/TPGS micelles. This smart drug delivery system aims to targeted delivery and acid-sensitive release of the FB15 to hypoxic and acidic tumor sites with CAIX overexpressing. In our strategy, the AZA-P188 was synthesized by introducing carboxylated P188 onto AZA through an acid-labile amide bond for targeting CAIX. The ionizable sulfonamide bond of AZA-P188 has pH-responsive properties and allows FB15 release triggered by tumor acidity

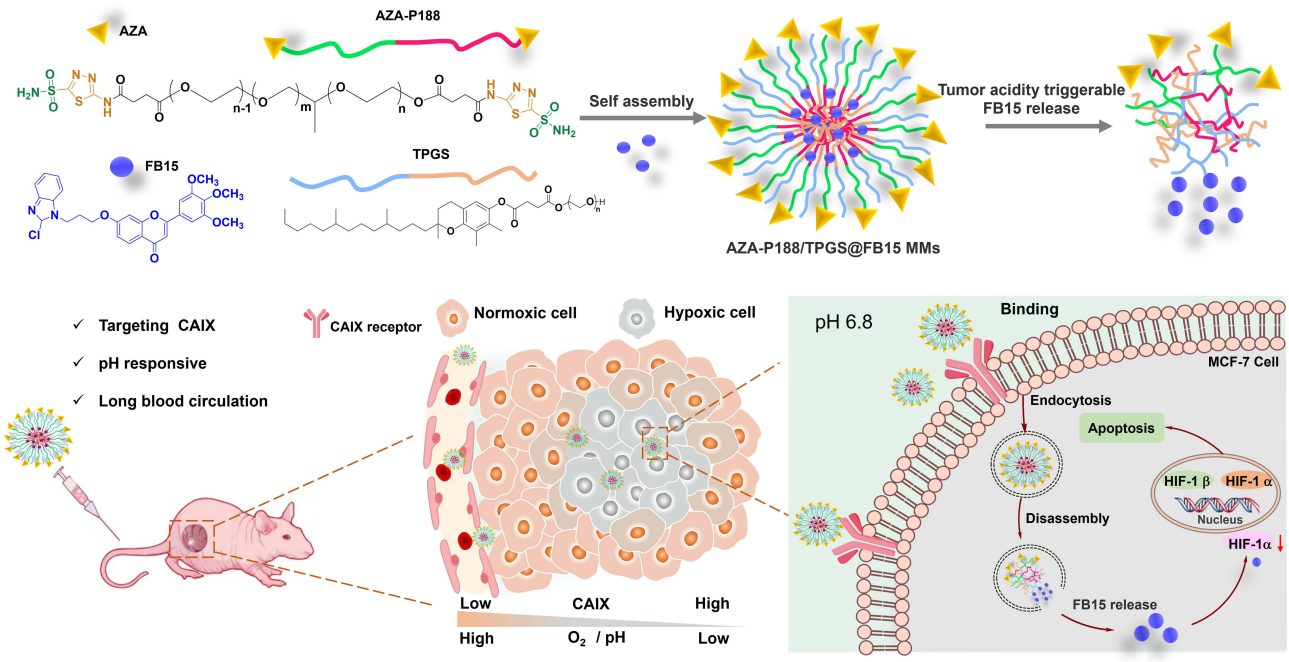

Scheme 1 Schematic illustration of smart (CAIX targetable and pH-responsive) nano-mixed micelles named AZA-P188/TPGS@FB15 Micelles for efficient anti-breast cancer.

microenvironment. TPGS forms self-assembled mixed micelles with AZA-P188 to improve the drug loading rate and stability and prolong blood circulation time. Subsequently, FB15 was encapsulated into the hydrophobic inner domains of AZA-P188/TPGS mixed micelles through the electrostatic interaction. After nanoparticle preparation, we investigated the physicochemical characteristics and biological properties of AZA-P188/TPGS@FB15 micelles, including the morphology, particle size, Zeta potentials, in vitro drug release, cellular uptake, and cytotoxicity. Additionally, its anti-tumor effects, pharmacokinetic and tissue distributions were further investigated in vivo. By exploiting the hypoxic and acidic microenvironment of tumor, the AZA modification nanocarrier system not only maximizes FB15 delivery to hypoxic tumor sites for exerting the glycolysis-blocking effect but also achieves rapid drug release under tumor acidic conditions (Scheme 1). The designed FB15-loaded targeted micelles demonstrated high efficacy in inhibiting tumor growth, providing a viable strategy to drive forward the clinical translation of such a novel candidate for hypoxic breast cancer and other solid tumors chemotherapy treatment.

Materials and Methods

Materials

The model drug FB-15 was obtained by employing a previously established method.[16] Acetazolamide (AZA), D-α-Tocopherol polyethylene1000 succinate (TPGS), and Poloxamer 188 (P188) were acquired from Haohong Pharmaceutical Co., Ltd, (Shanghai, China). Synthesis-related raw materials and catalysts, including N-hydroxysulfosuccinimide (NHS) and 1-Ethyl-3-[3-dimethylaminopropyl] carbodiimide hydrochloride (EDC), were obtained from Jingchun Reagent Co., Ltd (Shanghai, China). Dulbecco's modified eagle's medium (DMEM) was purchased from Gibco (USA). 4-6-diamidino-2-phenylindole (DAPI), fetal bovine serum (FBS), Methyl Thiazolyl Tetrazolium (MTT), and trypsin were acquired from Beyotime Biotechnology Co., Ltd (Shanghai, China). Human breast cancer cell lines MCF-7 were supplied by Shanghai Institute of Cellular Biology of Chinese Academy of Sciences. Sprague-Dawley (SD) rats (225 ± 25 g) and female BALB/c nude mice (20 ± 2 g, 4–5 weeks old) were acquired from Hunan Silaikejingda Experimental Animal Co., Ltd (Changsha, China).

Synthesis of AZA-P188

The synthesis of acetazolamide-amine (AZA-NH_2) from acetazolamide (AZA) by acid hydrolysis was conducted through acid hydrolysis, following previous described method.[27–29] This procedure involved adding acetazolamide (3.00 g, 13.34 mM) to a solution of hydrochloric acid (70.00 mM) in 70 mL, and stirring the liquid for 3 h under reflux condition. Column chromatography (CHCl3/MeOH: 100/0 to 70/30) was used to purify the resultant crude material in order to obtain the product 1,3,4-thiadiazole monohydrochloride (5-amino-2-sulfamoyl).[30]

A mixture of P188 (9.00 g), succinic anhydride (SA, 0.54 g), DMAP (0.27 g) and 0.5 mL triethylamine was co-dissolved in 30 mL of dioxane to synthesize the carboxylated P188. The solution was thoroughly mixed by magnetic stirring and allowed to react at room temperature for 24 h. The resulting mixed liquid was transferred to a dialysis bag with a relative molecular weight cutoff of 3500 Da, and the dialysis was performed with distilled water for 72 h. To effectively remove the organic solvent from the mixture, the dialysis buffer was replaced every 6 h during the initial 24 h, and the dialysis buffer was exchanged every 12 h for the following 48 h. The carboxylated P188 (CT-P188) was then obtained as a white powder through lyophilization.

Afterward, a solution of CT-P188 (1.5 g) and AZA-NH_2 (300 mg) in distilled water was prepared, and EDC (2.07 g) and NHS (1.03 g) were added to the mixed solution. The reaction was carried out with stirring for 24 h at ambient temperature. Subsequently, the resulting product was dialyzed using distilled water for 72 h, with regular water changes every 24 h. Finally, the mixture was subjected to freeze-drying to obtain a new polymer powder, AZA-P188.

Preparation of FB15-Loaded Micelles

FB15-loaded micelles were conducted using a filming-rehydration method. Briefly, different proportions of FB15 (2.5 mg, 5.0 mg, 10.0 mg), P188 (5.0 mg) and TPGS (145.0 mg) were dissolved in absolute ethyl alcohol in a round-bottom flask. The ethyl alcohol was evaporated under pressure at 50°C to form a uniform transparent film. Next, 5 mL of sterile saline (pH 7.4) was added to hydrate the lipid film at 25°C. The hydrated film was centrifuged at 4000 rpm for 10 min to obtain the mixed micelles (P188/TPGS@ FB15 Micelles). To prepare acetazolamide-functionalized micelles (AZA-P188/TPGS@FB15 Micelles), the same method was used with the substitution of P188 with AZA-P188.

Characterization of FB15-Loaded Nano-Micelles

The particle diameter and ζ-potential of FB15-loaded micelles were characterized by dynamic light scattering (90Plus PALS, Brookhaven Instrument, USA). The morphologic image of P188/TPGS@FB15 and AZA-P188/TPGS@FB15 micelles was captured by Transmission electron microscopy (TEM, FEI, USA). A series of feed ratios of TPGS to P188 were screened for their influence on loading capacity (LC) and encapsulation efficiency (EE) at a fixed FB15 dose of 5 mg. In brief, the AZA-P188/TPGS@FB15 micelles were ultrasound treated for 10 min dissolving in four-fold volumetric methanol. The content of FB15 was detected by HPLC (Waters, USA) on an ultimate XB-C18 column at 30 °C. The methanol and purified water (85:15, v/v) was used as the mobile phase in an isocratic elution. The standard curve of FB15 was established by measuring the absorbance of pure series concentration FB15 at 364 nm. Then, the LC and EE of FB15-loaded micelles were measured by the standard curve of FB15.

Drug Release Study In vitro

The release behavior of FB15 in vitro was evaluated using the dialysis method. Briefly, free FB15 and AZA-P188/TPGS@FB15 micelles with an equal amount of FB15 (50 μg) were dispersed in 2 mL of normal saline and then transferred into dialysis bags with 3500 Da molecular weight cut off (MWCO). The dialysis bags were then immersed in 30 mL release medium (PBS, 10 mM, pH 5.6, 6.8 and 7.4 with Tween-80) with gentle shaking (100 rpm) at 37 °C. At specified time intervals (0.5, 1, 2, 4, 6, 8, 10, 12, 24, 48 and 72 h), 1000 μL of release medium was collected, and 1000 μL of fresh medium was replenished. The content of FB15 was quantified by the HPLC method as described above.

In vitro Cytotoxicity Assay

The cytotoxicity was examined using MTT colorimetric assay. In short, MCF-7 cells were inoculated into 96-well plates. Following a 12-hour incubation, the cells were exposed to varying doses of free FB15, FB15-loaded micelles, and blank micelles in DMEM. After incubation for 24 h or 48 h, 20 μL of MTT solution (5 mg/mL) was added for continuous incubation for 4 h. The absorbance of each well at 490 nm was detected using the microplate reader.

In vitro Cell Uptake Study

MCF-7 cells in exponential growth phase were seeded into 6-well plates at a density of 1×10^5 cells per well. After incubation for 24 h to attach wall, the cells were incubated with gradient concentrations of Rhodamine 123 (Rh 123), P188/TPGS@Rh123 or AZA-P188/TPGS@Rh123 micelles for 2 h or 4 h incubation. For the receptor competition experiment, MCF-7 cells were preincubated with 2 mg/mL of AZA for 2 h before adding P188/TPGS@Rh123 or AZA-P188/TPGS@Rh123 micelles. This pretreatment aimed to investigate whether the cell uptake was mediated by AZA.

To visualize intracellular localization, the treated MCF-7 cells were fixed with 4% paraformaldehyde and the cell nuclei was stained with DAPI for 15 min. Intracellular localization was then observed with a fluorescence inversion microscope. In addition, to quantitatively analyze intracellular uptake, the treated MCF-7 cells were trypsinized and resuspended with PBS, and their fluorescence intensity was determined by flow cytometry.

Western Blot Assay

MCF-7 cells were seeded with 4×10^5 cells per well in a 6-well plate and treated with 6 μM of FB15 in different formulation of (Free FB15, AZA-P188/TPGS@FB15) for 48 h. Cell lysates were prepared by RIPA buffer (Servicebio, China) and then were centrifuged at 12,000 rpm for 15 min to collect total protein. 50 μg lysates proteins were treated with 8% sodium dodecyl-sulfate Polyacrylamide gel (SDS PAGE), transferred onto PVDF membranes (0.2 μm). The membranes were blocked with 5% skim milk in Tris-buffered saline with Tween 20 T (TBST) for 2 h at room temperature with gentle shaking, and incubated with primary antibodies against HK-II, PDK-1, CAIX or β-actin primary antibodies were incubated overnight at 4°C. Blots were washed with TBST (3 × 10 min) and then incubated with horseradish peroxidase-conjugated secondary antibody for 1 h at room temperature. Finally, the proteins were visualized using an enhanced chemiluminescence system (Tanon 5200, China).

Pharmacokinetics In vivo

The pharmacokinetic properties of AZA-P188/TPGS@FB15 micelles were contrasted with those of free FB15. Twelve male healthy SD rats were randomized into two experimental groups with 6 rats in each group. Two formulations of FB15 were injected intravenously into rats fasted overnight at an equivalent dose of 10 mg/kg (FB15). At predetermined time intervals (0.083, 0.167, 0.25, 0.5, 1, 2, 4, 8, 12, 24 h) from the retroorbital plexus of the rats and immediately centrifuged to get plasma. To determine the FB15 concentration in the plasma, 50 μL of the internal standard, chrysin (25 μg/mL), was mixed with 150 μL of the plasma and 2000 μL of methanol. The mixture was then vortexed for 5 min. Following centrifugation, the supernatant was recovered and the organic solvent was evaporated, and then residue was redissolved with 100 μL methanol for FB15 content analysis by HPLC.

The Tumor Targeting Ability In vivo

To observe the distribution of the targeted micelles, Rh123 was selected as a model drug because of its near-infrared fluorescent properties. Three experimental groups of female BALB/c nude mice bearing breast cancer were randomly assigned and were injected intravenously with free Rh123, AZA-P188/TPGS@Rh123, and P188/TPGS@Rh123 micelles at an equivalent dosage of 2 mg/kg (Rh123). In vivo fluorescence imaging was captured at 0, 1, 2 and 4 h with a Fusion FX7 fluorescence system. At four hours of intravenous administration, the mice were euthanized to collect the tumors tissue and the primary organs (spleen, heart, liver, kidneys, lungs) for ex vivo fluorescent imaging inspection.

Antitumor Effects of AZA-P188/TPGS@FB15 In vivo

To conduct the breast cancer-bearing tumor model, MCF-7 (2×10^6) cells in the logarithmic growth phase were injected subcutaneously into the mammary fat pads of 6-weeks-old female BALB/c nude mice. Twenty breast cancer mice were randomized into 4 experimental groups, 5 mice in each group. They were administered intravenously with 100 μL of saline, free FB15 (10 mg/kg), P188/TPGS@FB15 and AZA-P188/TPGS@FB15 micelles at doses of 10 mg/kg (FB15). Body weight and tumor volume were recorded every two days after injection. On the 12th day following administration, all mice were euthanized and then the tumor tissue and the major organs (kidneys, heart, liver, spleen, lungs) were detached, weighed, photographed, and stained with hematoxylin and eosin (H&E) for further analysis.

Assessment of Biochemical Parameters

Nine male healthy C57BL/J mice were randomized into three experimental groups with 3 rats in each group. They were administered intravenously with saline, free FB15 (10 mg/kg), and AZA-P188/TPGS@FB15 micelles at doses of 10 mg/kg (FB15). The drug was administered once every other day. After 10 days of the experimental period, all the animals were sacrificed and their blood was collected for the estimation of the liver and kidney function indexes. The blood samples were allowed to clot and centrifuged at 4000 rpm for 10 min and the obtained serum was used for further measurement of all the indicators. The aspartate aminotransferase (AST), alanine aminotransferase (ALT), UREA, creatinine (CREA) and uric acid (UA) in the serum were measured using commercial enzymatic kits (Huili, Changchun, China).

Statistical Analysis

All the data were expressed as mean ± SD of separate tests unless specified noted. Unpaired two-tailed Student's *T*-test was conducted to analyze significance of the data, and data with $p < 0.05$ was regarded as statistically significant (as calculated by GraphPad Prism 9.0).

Results and Discussion

Preparation and Characterization of AZA-P188/TPGS@FB15

This study aims to prepare acid-sensitive and CAIX-targeted nano-mixed micelles to improve the pharmacokinetics and pharmacodynamics of FB15. The synthesis route for AZA-P188 as dual-functional drug vehicles is depicted in Figure 1A. Firstly, carboxylated P188 was obtained through the reaction of P188 with 1,4-Dioxane catalyzed by 4-dimethylaminopyridine (4-DMAP) and triethylamine (TEA). Subsequently, acetazolamide (AZA) was subjected to hydrolysis under acidic conditions to expose amino group,[29] which was then conjugated with the carboxylated P188 through an amide bond using carbodiimide (EDC) and N-hydroxysuccinimide (NHS) as catalysts. The FTIR spectra of P188 and AZA-P188 are shown in Figure 1B. Notably, AZA-P188 exhibited a visible characteristic absorption peak of C=O of the –COOH group in AZA-P188 at 3400 cm^{-1}, 1650 cm^{-1}, and 1582 cm^{-1}, confirming the successful conjugation.

Additionally, ^{1}H NMR spectroscopy was employed to further characterize AZA-P188. The ^{1}H NMR results in Figure 1C revealed that the signals were at δ4.8 and 3.6~3.8 ppm, respectively corresponding to the resonance of the P188 protons (–CH– and $–CH_2–$). The signals of ^{1}H NMR spectra of AZA-P188 at δ 7.6~8.4 ppm derived from the resonance of the AZA proton. All data showed that AZA and P188 were conjugated successfully.

As a promising anti-tumor drug candidate, FB15 was obtained according to our previous report.[21] In the present study, FB15 was successfully loaded into AZA-P188/TPGS or P188/TPGS mixed micelles (P188/TPGS@FB15 or AZA-P188/TPGS@FB15) using a filming-rehydration method. TEM imaging verified the formation of homogeneous sphere-shaped nanoparticles, with average diameters of around 30 nm for AZA-P188/TPGS@FB15 micelles (Figure 1F). The hydrodynamic particle size measured by DLS was slightly larger due to the hydrated layer around the nanoparticles with a narrow particle size distribution (PDI < 0.3). The drug loading and encapsulation efficiency of AZA-P188/TPGS@FB15 were found to be 3.16% ± 0.73% and 94.57% ± 2.46%, respectively, as determined by HPLC analysis.

The zeta potential of P188/TPGS@FB15 and AZA-P188/TPGS@FB15 micelles was −16.47 ± 0.21 mV and −18.51 ± 0.34 mV respectively, facilitating the micellar solutions of stability and high biocompatibility (Figure 1D and E). Interestingly,

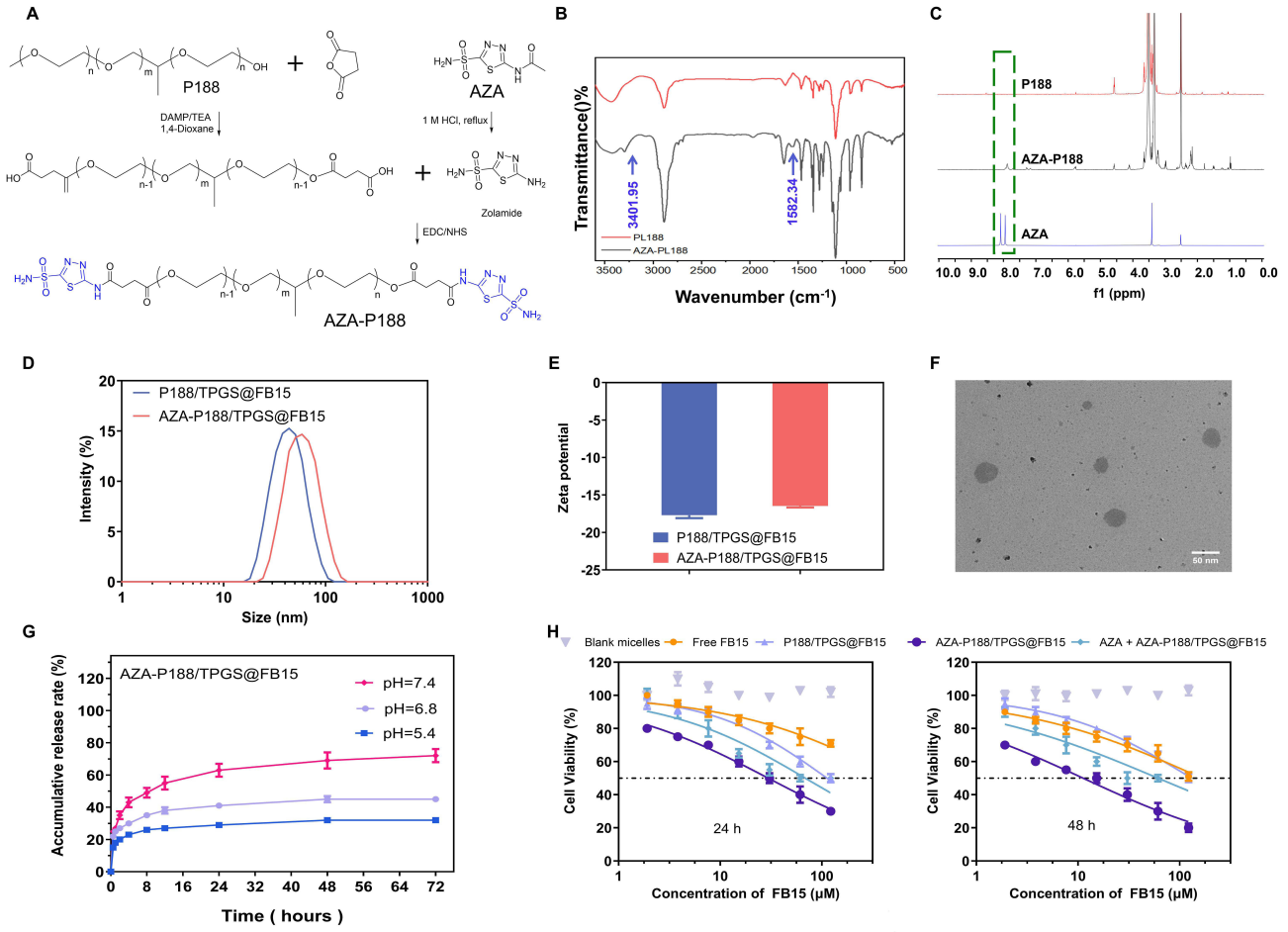

Figure 1 Preparation and characterization of the AZA-P188/TPGS@FB15 micelles (**A**) Synthesis scheme of AZA-P188. (**B**)FT-IR spectra of P188 and AZA-P188, respectively. (**C**) ^{1}H NMR spectrum of P188, AZA-P188 and AZA, respectively. (**D**) The particle size distributions and (**E**) Zeta potential of the P188/TPGS@FB15 and AZA-P188/TPGS@FB15 Micelles. (**F**) TEM image of AZA-P188/TPGS@FB15 Micelles. (**G**) The release curve of the AZA-P188/TPGS@FB15 at different pH in vitro. (**H**) The cell viability of MCF-7 incubated with FB15-loaded micelles after 24 h and 48 h.

when the pH of release buffer solution was dropped from 7.4 to 5.6, the particle size of AZA-P188/TPGS@FB15 significantly increased from 35.77 ± 2.14 nm to 454.11 ± 107.73 nm (Table 1), the Zeta potential of AZA-P188/TPGS@FB15 also significantly increased from −18.51 ± 0.34 mV to −2.08 ± 1.25 mV (Table 1). This may be ascribed to the more amino-protonation of both AZA-P188 and FB15 in Low-pH medium, resulting in enhanced hydrophilicity and/or electrostatic repulsion, leading to an increase in micelle particle size and Zeta potential. Another possible reason for the size increase might be the solubilization of FB15 under acidic conditions, weakening the electrostatic interactions between FB15 and the hydrophobic structural domains inside the AZA-P188/TPGS micelles.[31,32]

Release Behavior In vitro

The release properties of various FB 15 formulations were investigated in PBS with different acidity conditions added 1% SDS. As depicted in Figure 1G, the release of FB15 alone exhibited a rapid and complete release within the initial 3

Table 1 Characterization of AZA-P188/TPGS@FB15 Micelles in PBS at Different pH Condition (Means ± SD, n = 3)

pH value	Particle diameter (nm)	PDI	ζ-potential (mV)
7.4	35.77 ± 2.14	0.12 ± 0.01	−18.51 ± 0.34
6.8	300.13 ± 60.14	0.49 ± 0.07	−3.50 ± 1.17
5.6	454.11 ± 107.73	0.54 ± 0.09	−2.08 ± 1.25

hours at pH 7.4, while FB15-loaded micelles demonstrated a significantly slower release rate, displaying two-phase release patterns of an incipient rapid release followed by a constant release. For AZA-P188/TPGS@FB15 micelles, the incipient rapid release of FB15 may be ascribed to its physical absorption on the surface of FB15-loaded micelles, while the constant release could be attributed to encapsulation of the FB15 in the AZA-P188/TPGS micelles core.

The cumulative release rates of FB15 from the targeted nano-mixed micelles within the 72 h were 75.16% ± 0.89%, 40.11% ± 1.43%, and 25.30% ± 3.21% in the release medium at pH 5.6, 6.8, and 7.4, respectively. Notably, in comparison to pH 7.4 media (simulating physiological environment), AZA-P188/TPGS@FB15 micelles exhibited an enhanced release rate in the media with pH 5.6 and 6.8 (simulating acidic tumor microenvironment). It is possible that the protonation of the tertiary amine moiety of FB15 under acidic conditions led to increase the solubilization of FB15 and weaken the electrostatic interaction between hydrophobic FB15 and the hydrophobic core of AZA-P188/TPGS micelles, causing the acidic-sensitive release characteristics of AZA-P188/TPGS@FB15 micelles, with an increasing FB15 release rate with decreasing pH. Hence, FB15 release rate was higher at pH 5.4 than at pH 7.4 and at pH 6.8. The acidic-sensitive release characteristics of AZA-P188/TPGS@FB15 micelles, with an increasing FB15 release rate with decreasing pH, may be induced by the protonation of the tertiary amine moiety of FB15 under acidic conditions, which increased the solubilization of FB15 and weakened the electrostatic interaction between hydrophobic FB15 and hydrophobic core of AZA-P188/TPGS nano micelles.[33,34] Moreover, this behavior may be also caused by the breakage of the acid-sensitive ionizable sulfonamide bond of AZA-P188 under acidic conditions,[35,36] which triggers the higher release of FB15. The reduction of negative charge on AZA-P188/TPGS@FB15 micelles at acidic pH (Table 1) may facilitate cellular uptake and efficient intracellular drug release, potentially enhancing therapeutic efficacy.[37,38]

Effects of AZA-P188/TPGS@FB15 on Cell Viability

MTT assays were performed with CAIX-positive cell-line MCF-7 to assess the cytotoxicity of FB15-loaded micelles in culture medium. As depicted in Figure 1H, the cell viabilities both exceeded 95% for the vehicles, which demonstrated that the vehicles possessed enhanced biocompatibility. Free FB15 and FB15-loaded micelles showed concentration-dependent cytotoxicity towards MCF-7 cells for 24 hours and 48 hours. It was worth noting that AZA-P188/TPGS@FB15 micelles (IC50 = 11.2 ± 1.9 μM) demonstrated higher cytotoxicity than P188/TPGS@FB15 micelles (IC50 = 131.3 ± 8.5 μM) and free FB15 (IC50 = 165.9 ± 15.4 μM) in MCF cells after 48h of treatment (Figure 1H and Table 2). This substantially enhanced cytotoxicity suggests that the AZA-P188/TPGS@FB15 nanoparticles effectively delivered FB15 to the target cells, potentially improving the therapeutic outcome.

Cell Targeting Ability of Rh-123 Labeled AZA-P188/TPGS

One merit for AZA modification in AZA-P188/TPGS@FB15 is its ability to target CAIX overexpressed cancer cells. To verify the ability of AZA-P188/TPGS micelles for CAIX-mediated targeted of FB15, we prepared the Rh123 labeled P188/TPGS or AZA-P188/TPGS micelles and investigated the cellular uptake using MCF-7 cell with CAIX overexpressing as an example.

The Rh123 with green fluorescence was applied for the localization of nano micelles, and the DAPI with blue fluorescence was applied for the localization of nuclei. Intracellular localization was then observed with a fluorescence inversion microscope. After co-incubation with free Rh123, Rh123-labeled micelles for 2 h, only weak green fluorescence was detected in the free Rh123 group, while strong cytoplasmic green fluorescence could be observed in the Rh123-labeled micelles group, indicating effective uptake of Rh123-labeled P188/TPGS or AZA-P188/TPGS micelles by MCF-7 cells (Figure 2A and B). The

Table 2 The IC50 Values on MCF-7 Cells Incubated with Free FB15 and FB15 Loaded Micelles After 24 h and 48 h (Means ± SD, = 3)

Sample	IC50	
	24 h	48 h
P188/TPGS@FB15	529.5 ± 21.2 μM	165.9 ±15.4 μM
P188/TPGS@FB15	112.6 ± 15.6 μM	131.3 ± 8.5 μM
AZA-P188/TPGS@FB15	29.7 ± 4.3 μM	11.2 ± 1.9 μM
AZA + AZA-P188/TPGS@FB15	68.8 ± 6.9 μM	61.2 ± 7.3 μM

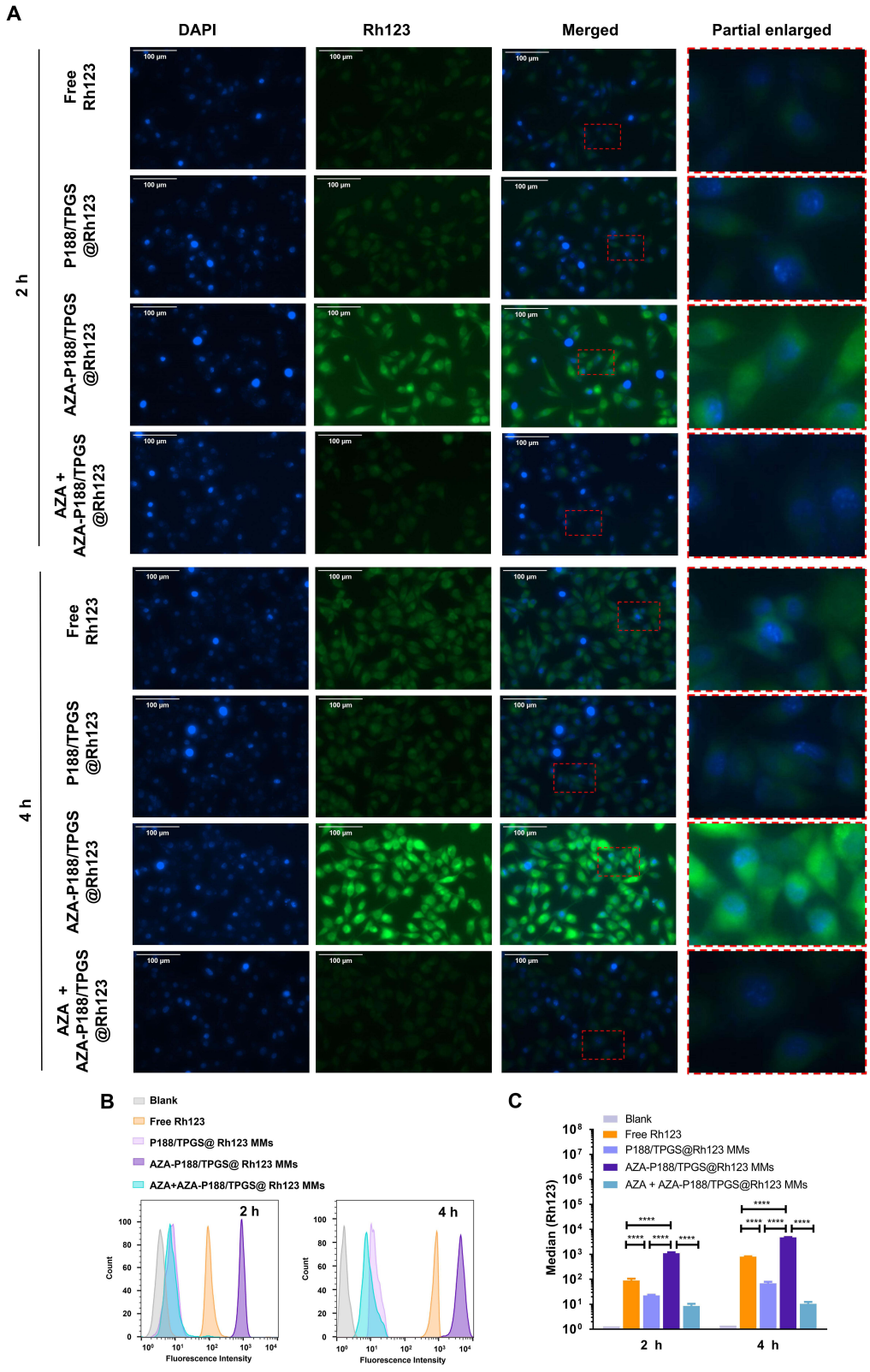

Figure 2 (**A**) Fluorescence images of MCF-7 cells following 4 h and 12 h with free Rh123, and P188/TPGS@Rh123 or AZA-P188/TPGS@Rh123 micelles (Blue: DAPI; Green: Rh123); (**B**) Fluorescence quantitative images of MCF-7 cells subjected to free Rh123, and P188/TPGS@Rh123 or AZA-P188/TPGS@Rh123 micelles by flow cytometry. (**C**) Statistical analysis of fluorescence intensity (n = 3); The data were analyzed using unpaired two-tailed Student's *t*-test. Data were expressed as mean ± SD (n = 3), probability value of $^{****}p < 0.0001$ was considered significant.

fluorescence of Rh123 labeled AZA-P188/TPGS micelles group was slightly stronger than that of Rh123 labeled P188/TPGS group, and this difference became more pronounced at 4 hours (Figure 2A and B). These findings suggested that AZA facilitates the entry of P188/TPGS into the cells and enhances the micelles uptake. To further investigate whether AZA-P188/TPGS micelles entry into cells through receptor-mediated endocytosis, we performed receptor competition experiments using flow cytometry. We used free AZA to pre-saturate the CAIX receptor on the cell surface to evaluate the uptake of the micelles in the presence or absence of competitive inhibitor.[25,39] After pretreating the MCF-7 cells with an excess amount of AZA (2 mg/mL), the fluorescence intensity of AZA-P188/TPGS@ Rh123 was only 6.1% of that pretreated without AZA (co-incubation for 4 h, Figure 2C). This result indicates that the CAIX receptor on the cell membrane was mostly bound to free AZA,[39] leading to significant inhibition of AZA-P188/TPGS micelles uptake. Overall, these findings demonstrate that Rh123-labeled AZA-P188/TPGS were endocytosed into the cells through a CAIX-mediated manner.

The Anti-Tumor Mechanism of AZA-P188/TPGS@FB15 Micelles

In our previous studies, FB15 significantly inhibited the glycolytic enzymes HK-II, PFKP and PDK-1 at the molecular level in MGC-803 cells.[17] To further validate the targeting mechanism of AZA-P188/TPGS@FB15 micelles, the effect of AZA-P188/TPGS@FB15 on CAIX, HK-II and PDK-1 expression was explored through Western blotting. As shown in Figure 3, the expression level of CAIX in the AZA-P188/TPGS@FB15 group was significantly lower than that in the blank control group and FB15 group, which demonstrated AZA-P188/TPGS@FB15 have a significant inhibitory effect on CAIX at the molecular level. Furthermore, AZA-P188/TPGS@FB15 downregulated the expression of PDK-1 and HK-II significantly, compare with free FB15. These findings suggested that AZA modification nanocarrier system enhances FB15 delivery to hypoxic tumor sites by targeting CAIX, thereby promoting the glycolysis-blocking effect of FB15 in MCF-7 tumor cells.

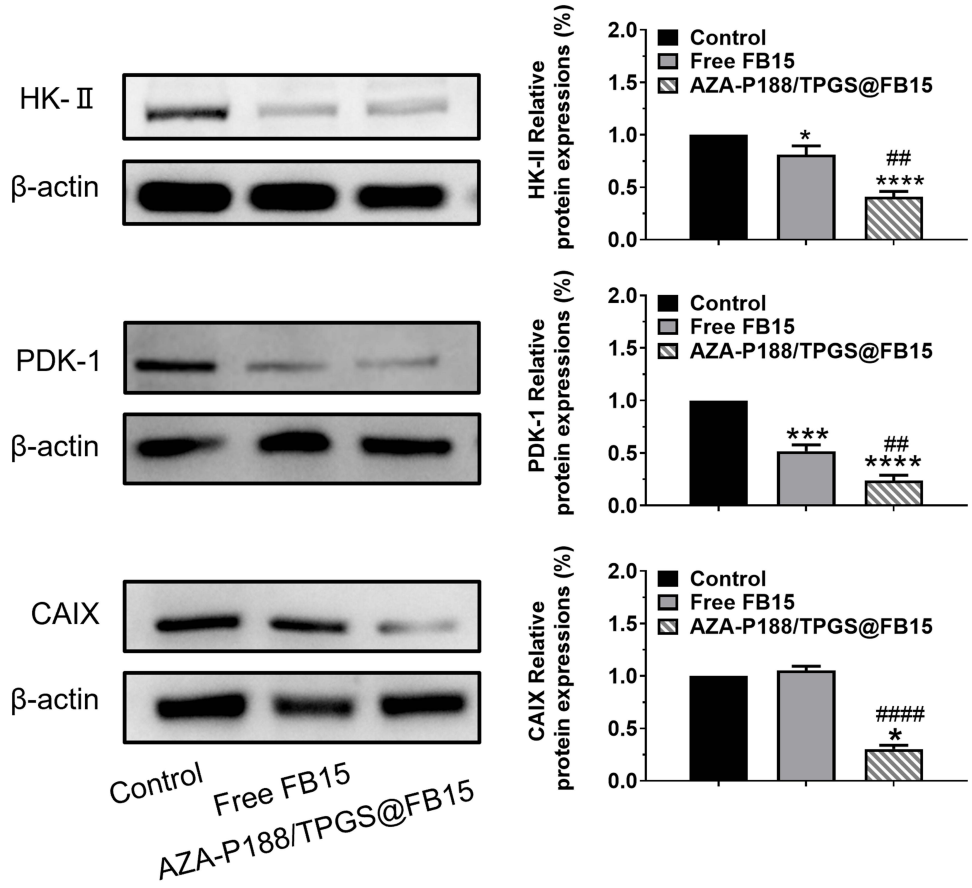

Figure 3 The expression of HK-II, PDK-1 and CAIX in MCF-7 tumor cells (n = 3; *p < 0.05 and ***p< 0.001 or ****p< 0.0001 compared with the control group; ##p < 0.01 and #####p < 0.0001 compared with the free FB15 group).

Table 3 Plasma Pharmacokinetics Parameters of FB15 (10 Mg/Kg) After Intravenous Administration of Free FB15 and AZA-P188/TPGS@FB15 Micelles to Rats (Means ± SD, n = 6)

Pharmacokinetic parameter	Free FB15	AZA-P188/ TPGS@FB15
AUC_{0-t} (μg/L·h)	174.11 ± 13.06	1514.15 ± 54.12***
$AUC_{0-\infty}$ (μg /L·h)	192.09 ± 16.20	1535.28 ± 65.17***
MRT_{0-t} (h)	2.76 ± 0.53	6.45 ± 1.04***
$MRT_{0-\infty}$(h)	3.70 ± 0.76	8.59 ± 1.53***
$t_{1/2z}$(h)	2.98 ± 0.03	4.00 ± 0.13***
$CL_{z/F}$(L/h/kg)	44.97 ± 5.51	5.99 ± 1.76***
C_{max}(mg/L)	0.22 ± 0.02	0.38 ± 0.06***

Notes: Significant differences from free FB15 were denoted as ***$p < 0.001$.

Pharmacokinetics Studies of AZA-P188/TPGS@FB15 Micelles

We evaluated the main pharmacokinetic properties of AZA-P188/TPGS@FB15 micelles in comparison to free FB15. As shown in Table 3 and Figure 4, the area under the curve ($AUC_{0-\infty}$) of FB15 after intravenous administration in AZA-P188/TPGS@FB15 micelles (1535.28 ± 65.17 h·mg/mL, ~8-fold) was profoundly higher than that of free FB15 (192.09 ± 16.20 h·mg/mL), indicating a substantially enhanced absolute bioavailability with this micellar formulation. The mean residue time ($MRT_{0-\infty}$) of FB15 in the AZA-P188/TPGS@FB15 micelles (8.59 ± 1.53 h, ~2.3-fold) was profoundly longer than that of FB15 alone (3.70 ± 0.76 h). Furthermore, the clearance rates (CL) of FB15 in the AZA-P188/TPGS@FB15 micelles (5.99 ± 1.76 L/h/kg) were lower than those of the free FB15 (44.97 ± 5.51 L/h/kg). These results demonstrated that the encapsulation of FB15 in the targeted nano micelles remarkably enhanced its pharmacokinetic profile, consistent with the reports that nano-mixed micelles would significantly change the blood circulation time and bioavailability.

In vivo Biodistribution Analysis

After characterizing the intracellular targeting performance, we used Rh123 was loaded into P188/TPGS or AZA-P188/TPGS micelles to visualize the performance of biodistribution in vivo. Both free Rh123 and Rh123-loaded micelles were administrated intravenously into the MCF-7 tumor-bearing BALB/c nude mice, and the fluorescent images of these mice were captured at different time intervals with a Fusion FX7 fluorescence system. Both Rh123 alone and Rh123-loaded nano-micelles were rapidly distributed throughout the body of tumor-bearing mice at 1 h post-injection. Encouragingly, at four hours post-injection, the

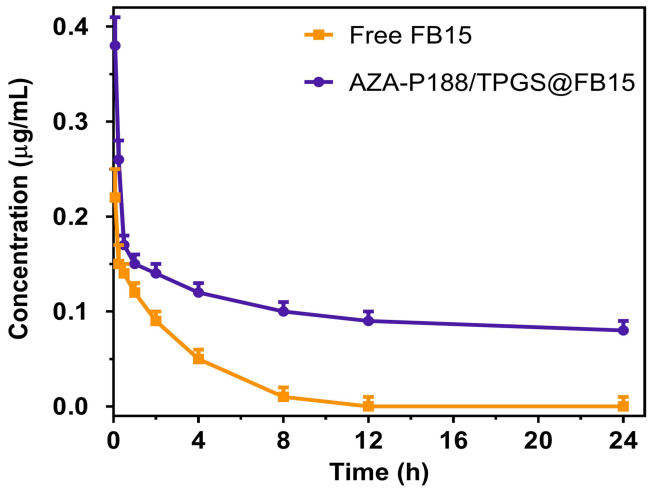

Figure 4 The FB15 mean plasma concentration-time profiles of the free FB15, the AZA-P188/TPGS@FB15 micelles at a dose of 10 mg/kg FB15 in rats. Data were presented mean ± SD (n = 6).

fluorescence distribution in mice injected with AZA-PL188/TPGS@Rh123 micelles was almost all concentrated at the tumor site, while free Rh123 and non-targeted P188/TPGS@Rh123 showed intense fluorescence distribution throughout the body (Figure 5A).

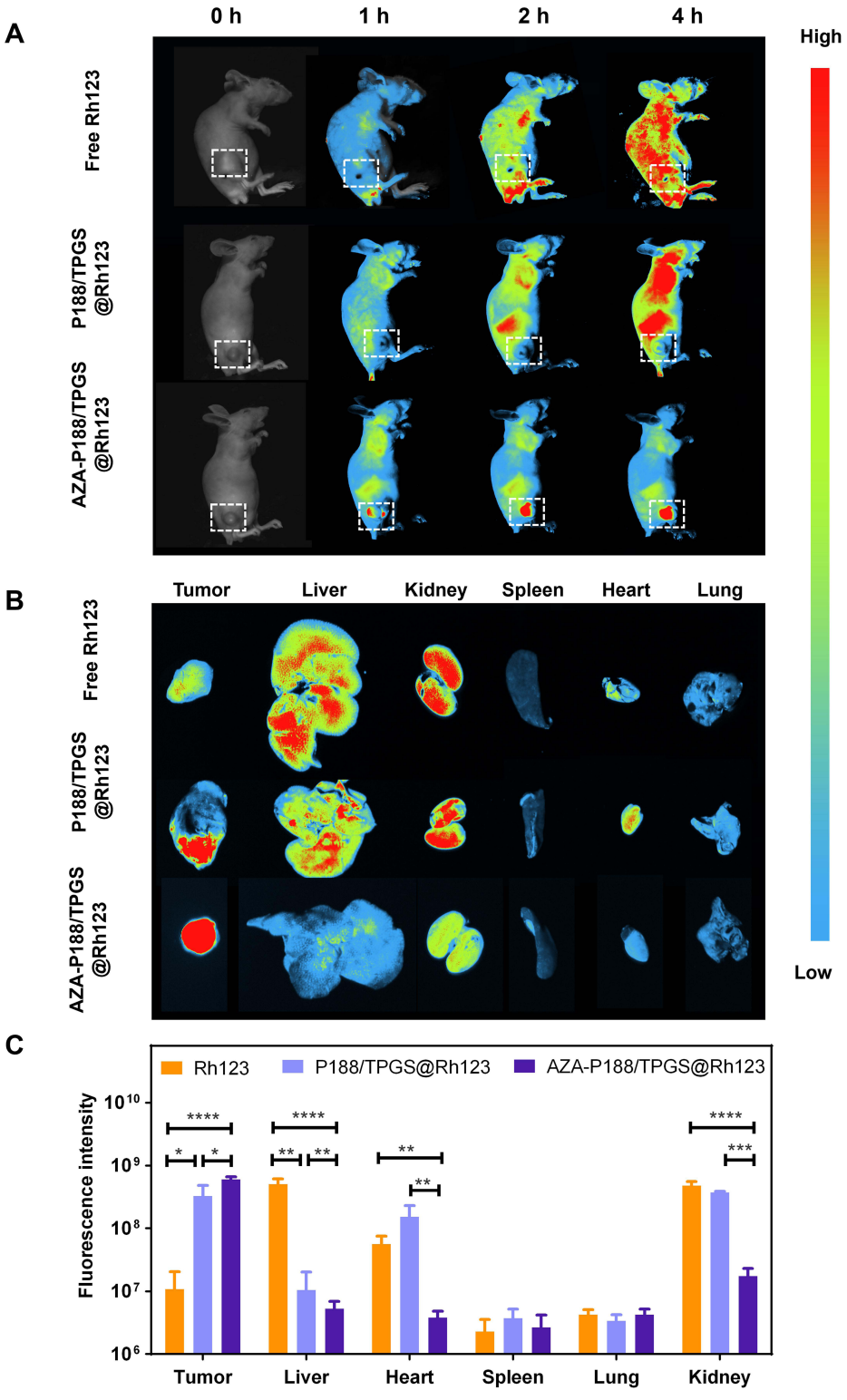

Figure 5 (**A**) In vivo biodistribution of free Rh123 and Rh123-loaded micelles for 0 h, 1 h, 2 h and 4 h. (**B**) Ex vivo tissue distribution of free Rh123 and Rh123-loaded micelles for 4 h. (**C**) Fluorescence intensity analysis of ex vivo tissue (n = 3); The data were analyzed using unpaired two-tailed Student's *t*-test. Data were expressed as mean ± SD (n = 3). A probability value of **p* <0.05, ***p* <0.01, ****p* <0.001 or *****p* <0.0001 was considered significant.

To further substantiate this observation, the tumor tissue and major organ were excised from tumor-bearing mice, and fluorescence intensity was analyzed ex vivo for free Rh123, P188/TPGS@Rh123, and AZA-P188/TPGS@Rh123 micelles (Figure 5B and C). In contrast to the free-Rh123 formulation, both nano-mixed micelles manifested the increased fluorescence intensities accumulation in tumor tissues, presumably resulting from the enhancement of permeation and the retention effect of nano-sized micelles in the tumor sites.[40] Remarkably, the fluorescence of AZA-P188/TPGS@Rh123 was significantly stronger in the tumor site than that of the P188/TPGS@Rh123 micelles. These results indicate that the AZA-P188/TPGS@Rh123 micelles achieved superior tumor-targeting efficiency compared to the P188/TPGS@Rh123, which may be primarily ascribed to more endocytosis mediated by the receptor-ligand interaction.[25,40] The excellent tumor-targeting capability of AZA-P188/TPGS@Rh123 micelles holds great promise for targeted drug delivery to CAIX-overexpressed cancer cells.

In vivo Anticancer Activity

Since AZA-P188/TPGS@FB15 micelles exhibited superior cytotoxicity against MCF-7 cells, improved pharmacokinetic properties in rats, and encouraging targeting ability to tumors in comparison to free FB15, the anti-tumor ability in vivo of the FB15-loaded micelles was assessed by MCF-7 bearing tumor model. Tumor weight in the free FB15 group was not obviously different from the saline control group, while both non-targeted or targeted FB15 nanomedicine inhibited tumor growth significantly in contrast to the saline control and free FB15, which may be ascribed to the enhanced FB15 pharmacokinetic properties and permeability and retention (EPR) effect of nano-size micelles (Figure 1G and Table 3). Notably, the targeted FB15-loaded micelles exerted the highest the inhibitory effects on the tumor in comparison to the non-targeted FB15-loaded micelles and free FB15 group ($p < 0.001$), which was evident from the slowest tumor growth rate and the smallest tumor volume observed in the AZA-P188/TPGS@FB15 group (Figure 6B and C). Among three FB15 formulations, the tumor cells in AZA-P188/TPGS@FB15 group had most serious apoptosis and necrosis, according to H&E staining of tumor tissues (Figure 6D). These results may be attributed to the active targeting of CAIX receptors by AZA ligands and the pH-sensitive rapid release of FB15 from these micelles under tumor acidic conditions. In addition, glomerular atrophy was observed in the free FB15 group, while both FB15 nano-formulation did not cause significant pathology in the major organs and not observe a significant drop in body weight of the tumor-bearing mice during the therapeutic period over the saline group (Figure 6A–D). This suggests that FB15 may cause some pathological damage to the kidneys of mice. Moreover, we evaluated the effects of FB15 and AZA-P188/TPGS@FB15 on liver and kidney function indexes in healthy C57BL/J mice. As shown in Table 4, the mice of FB15 group exhibited significantly ($p < 0.05$) higher AST, UREA, CREA and UA compared with the normal control group, which validated the nephrotoxicity of FB15. It is worth noting that there was no significant difference between the AZA-P188/TPGS@FB15 group and the normal control group for these biochemical parameters of liver and kidney function. These results preliminarily indicated that the encapsulation of AZA-P188/TPGS improves FB15 biocompatibility in mice. Overall, these findings suggested that the AZA-P188/TPGS@FB15 micelles exert a better anti-breast cancer efficacy in vivo accompanying lower systemic toxicity.

Conclusions

In this study, the authors successfully constructed a CAIX-targeted nano-delivery system loaded with the promising HIF-1 inhibitor FB15 (AZA-P188/TPGS@FB15) for targeted therapy of breast cancer and other solid tumors. The AZA-P188/TPGS@FB15 micelles exhibited responsive drug release in an acidic environment and accumulated preferentially in tumor tissues. The results showed that AZA-P188/TPGS@FB15 micelles exhibited higher cellular uptake and better inhibitory effects in vitro, in contrast to free FB15 and the non-targeted P188/TPGS@FB15 micelles. The AZA-P188/TPGS micelles could achieve superior drug accumulation in tumor tissues compared with the non-targeted micelles. AZA modification nanocarrier system enhances FB15 delivery to hypoxic tumor sites by targeting CAIX, thereby promoting the glycolysis-blocking effect of FB15 in tumor cells. Encapsulation of FB15 in AZA-P188/TPGS has also improved the pharmacokinetics of FB15. In an MCF-7 tumor model, AZA-P188/

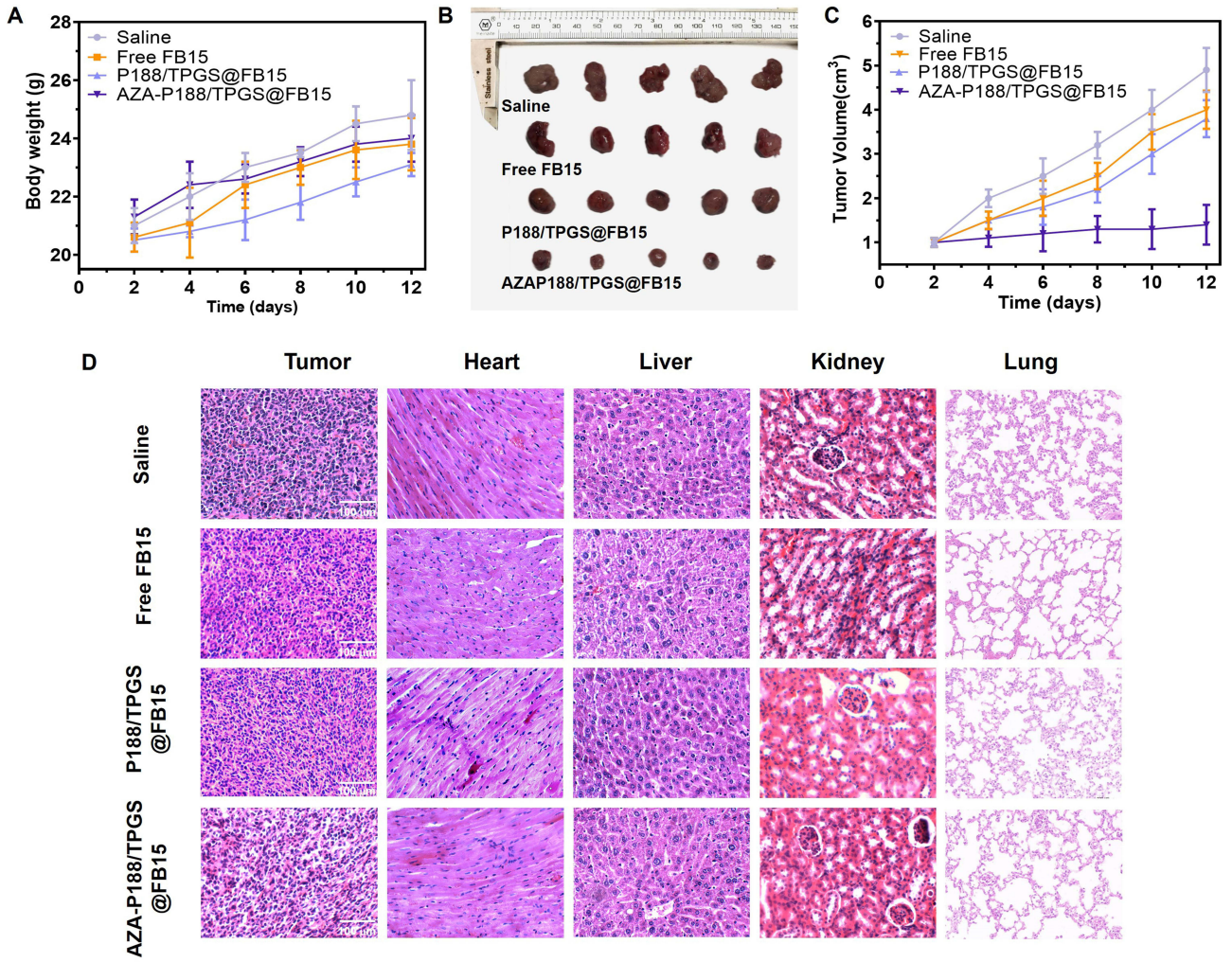

Figure 6 In vivo experiments. (**A**) The body weight change curve of nude mice over a period of 12 day; (**B**) Photographs showing tumor inhibition after different treatments; (**C**) Tumor growth curves after treatment with saline, free FB15, P188/TPGS@FB15 and AZA-P188/TPGS@FB15 micelles; (**D**) Histopathological analysis of the tumor tissues, heart, liver, kidney stained with hematoxylin after treatment with saline, free FB15, P188/TPGS@FB15, and AZA-P188/TPGS@FB15 micelles.

TPGS@FB15 inhibited tumor glycolysis and exerted the best tumor suppressive effect, which may be ascribed to the preferential accumulation and acid-responsive release of FB15 in the tumor environment via CAIX-targeting delivery system. Overall, AZA-P188/TPGS@FB15 micelles exhibit excellent tumor-targeting capabilities and superior antitumor efficacy, providing a viable candidate for targeted therapy to hypoxic breast cancer and other solid tumors.

Table 4 Effects of Free FB15 and FB15-Loaded Micelles on ALT, AST, UREA, CREA and UA in C57BL/6J Mice (Means ± SD, n = 3)

Group	ALT (U/L)	AST (U/L)	UREA (mM)	CREA (mM)	UA (mM)
Normal control	47.25 ± 1.02	120.61 ± 20.24	24.31 ± 5.4	14.85 ± 0.31	14.85 ± 0.31
Free FB15	55.11 ± 11.86	202.98 ± 44.16*	35.15 ± 1.11*	20.99 ± 1.82**	20.99 ± 1.82*
AZA-P188/TPGS@FB15	44.59 ± 8.35	121.11 ± 16.77	25.07 ± 1.85	15.41 ± 2.14	15.41 ± 2.14

Notes: Significant differences from normal control were denoted as *$p < 0.05$, **$p < 0.01$.

Ethics of Animals

All animal experimentations were authorized by the Institutional Animal Care and Ethics Committee of the affiliated Nanhua hospital, University of South China (Approval No. 2021-ky-130) and performed in adherence with the principles and procedures of the National Institutes of Health (NIH) Guide for the Care and Use of Laboratory Animals and the Guidelines for Animal Treatment of University of South China. We fully respected the lives of laboratory animals, made every effort to minimize the number of experimental animals and alleviate their painfulness.

Acknowledgments

This research was funded by the Health Project of Health commission of Hunan Province, China (No. W20243180, No.20201914), the Hunan Provincial Natural Science Foundation of China (No.2022JJ40405, 2023JJ40602, 2023JJ40576), the NSFC of China (No.82304420). We also thanked the Hunan Provincial Key Laboratory of tumor microenvironment responsive drug research (No. 2019-56).

Disclosure

The authors report no conflicts of interest in this work.

References

1. Sung H, Ferlay J, Siegel RL, et al. Global cancer statistics 2020: GLOBOCAN estimates of incidence and mortality worldwide for 36 cancers in 185 countries. *CA Cancer J Clin*. 2021;71(3):209–249. doi:10.3322/caac.21660
2. Catalano V, Turdo A, Di Franco S, Dieli F, Todaro M, Stassi G. Tumor and its microenvironment: a synergistic interplay. *Semin Cancer Biol*. 2013;23(6 Pt B):522–532. doi:10.1016/j.semcancer.2013.08.007
3. de Heer EC, Jalving M, Harris AL. HIFs, angiogenesis, and metabolism: elusive enemies in breast cancer. *J Clin Invest*. 2020;130(10):5074–5087. doi:10.1172/JCI137552
4. Wicks EE, Semenza GL. Hypoxia-inducible factors: cancer progression and clinical translation. *J Clin Invest*. 2022;132(11). doi:10.1172/JCI159839
5. Chen Z, Han F, Du Y, Shi H, Zhou W. Hypoxic microenvironment in cancer: molecular mechanisms and therapeutic interventions. *Signal Transduct Target Ther*. 2023;8(1):70. doi:10.1038/s41392-023-01332-8
6. Wang GL, Jiang BH, Rue EA, Semenza GL. Hypoxia-inducible factor 1 is a basic-helix-loop-helix-PAS heterodimer regulated by cellular O2 tension. *Proc Natl Acad Sci*. 1995;92(12):5510–5514. doi:10.1073/pnas.92.12.5510
7. Zhao Z, Mu H, Li Y, Liu Y, Zou J, Zhu Y. Clinicopathological and prognostic value of hypoxia-inducible factor-1α in breast cancer: a meta-analysis including 5177 patients. *Clin Transl Oncol*. 2020;22(10):1892–1906. doi:10.1007/s12094-020-02332-8
8. Cao Q, Mushajiang M, Tang CQ, Ai XQ. Role of hypoxia-inducible factor-1α and survivin in breast cancer recurrence and prognosis. *Heliyon*. 2023;9(3):e14132. doi:10.1016/j.heliyon.2023.e14132
9. McAleese CE, Choudhury C, Butcher NJ, Minchin RF. Hypoxia-mediated drug resistance in breast cancers. *Cancer Lett*. 2021;502:189–199. doi:10.1016/j.canlet.2020.11.045
10. Bhattarai D, Xu X, Lee K. Hypoxia-inducible factor-1 (HIF-1) inhibitors from the last decade (2007 to 2016): a "structure-activity relationship" perspective. *Med Res Rev*. 2018;38(4):1404–1442. doi:10.1002/med.21477
11. Zhu ZY, Wang F, Jia CH, Xie ML. Apigenin-induced HIF-1α inhibitory effect improves abnormal glucolipid metabolism in AngII/hypoxia-stimulated or HIF-1α-overexpressed H9c2 cells. *Phytomedicine*. 2019;62:152713. doi:10.1016/j.phymed.2018.10.010
12. Yi X, Qi M, Huang M, Zhou S, Xiong J. Honokiol inhibits HIF-1α-mediated glycolysis to halt breast cancer growth. *Front Pharmacol*. 2022;13:796763. doi:10.3389/fphar.2022.796763
13. Martí-Díaz R, Montenegro MF, Cabezas-Herrera J, Goding CR, Rodríguez-López JN, Sánchez-Del-Campo L. Acriflavine, a potent inhibitor of HIF-1α, disturbs glucose metabolism and suppresses atf4-protective pathways in melanoma under non-hypoxic conditions. *Cancers*. 2020;13(1):102. doi:10.3390/cancers13010102
14. Hideshima T, Mitsiades C, Akiyama M, et al. Molecular mechanisms mediating antimyeloma activity of proteasome inhibitor PS-341. *Blood*. 2003;101(4):1530–1534. doi:10.1182/blood-2002-08-2543
15. Mooberry SL. Mechanism of action of 2-methoxyestradiol: new developments. *Drug Resist Updat*. 2003;6(6):355–361. doi:10.1016/j.drup.2003.10.001
16. Wang Z, Deng X, Xiong R, et al. Design, synthesis and biological evaluation of 3',4',5'-trimethoxy flavonoid benzimidazole derivatives as potential anti-tumor agents. *Medchemcomm*. 2018;9(2):305–315. doi:10.1039/C7MD00578D
17. Deng X, Pi Y, Li Z, et al. FB-15 inhibits MGC-803 cells growth by regulating energy metabolism. *Chem Biol Interact*. 2020;327:109186. doi:10.1016/j.cbi.2020.109186
18. Lou Y, McDonald PC, Oloumi A, et al. Targeting tumor hypoxia: suppression of breast tumor growth and metastasis by novel carbonic anhydrase IX inhibitors. *Cancer Res*. 2011;71(9):3364–3376. doi:10.1158/0008-5472.CAN-10-4261
19. Li Z, Jiang L, Chew SH, Hirayama T, Sekido Y, Toyokuni S. Carbonic anhydrase 9 confers resistance to ferroptosis/apoptosis in malignant mesothelioma under hypoxia. *Redox Biol*. 2019;26:101297. doi:10.1016/j.redox.2019.101297
20. Rezuchova I, Bartosova M, Belvoncikova P, et al. Carbonic anhydrase IX in tumor tissue and plasma of breast cancer patients: reliable biomarker of hypoxia and prognosis. *Int J Mol Sci*. 2023;24(5):4325. doi:10.3390/ijms24054325

21. Trastour C, Benizri E, Ettore F, et al. HIF-1alpha and CA IX staining in invasive breast carcinomas: prognosis and treatment outcome. *Int J Cancer*. 2007;120(7):1451–1458. doi:10.1002/ijc.22436
22. Janoniene A, Mazutis L, Matulis D, et al. Inhibition of carbonic anhydrase IX suppresses breast cancer cell motility at the single-cell level. *Int J Mol Sci*. 2021;22(21):11571. doi:10.3390/ijms222111571
23. Chafe SC, Vizeacoumar FS, Venkateswaran G, et al. Genome-wide synthetic lethal screen unveils novel CAIX-NFS1/xCT axis as a targetable vulnerability in hypoxic solid tumors. *Sci Adv*. 2021;7(35). doi:10.1126/sciadv.abj0364
24. Liu N, Lin Q, Zuo W, et al. Carbonic anhydrase IX-targeted nanovesicles potentiated ferroptosis by remodeling the intracellular environment for synergetic cancer therapy. *Nanoscale Horiz*. 2023;8(6):783–793. doi:10.1039/D2NH00494A
25. Janoniene A, Liu Z, Baranauskiene L, et al. A versatile carbonic anhydrase IX targeting ligand-functionalized porous silicon nanoplatform for dual hypoxia cancer therapy and imaging. *ACS Appl Mater Interfaces*. 2017;9(16):13976–13987. doi:10.1021/acsami.7b04038
26. Zhong C, Chen J, Ling Y, et al. Indocyanine green-loaded nanobubbles targeting carbonic anhydrase IX for multimodal imaging of renal cell carcinoma. *Int J Nanomed*. 2023;18:2757–2776. doi:10.2147/IJN.S408977
27. Ilies MA, Vullo D, Pastorek J, et al. Carbonic anhydrase inhibitors. Inhibition of tumor-associated isozyme IX by halogenosulfanilamide and halogenophenylaminobenzolamide derivatives. *J Med Chem*. 2003;46(11):2187–2196. doi:10.1021/jm021123s
28. Akocak S, Alam MR, Shabana AM, et al. PEGylated bis-sulfonamide carbonic anhydrase inhibitors can efficiently control the growth of several carbonic anhydrase IX-expressing carcinomas. *J Med Chem*. 2016;59(10):5077–5088. doi:10.1021/acs.jmedchem.6b00492
29. Tatiparti K, Sau S, Gawde KA, Iyer AK. Copper-free 'click' chemistry-based synthesis and characterization of carbonic anhydrase-IX anchored albumin-paclitaxel nanoparticles for targeting tumor hypoxia. *Int J Mol Sci*. 2018;19(3):838. doi:10.3390/ijms19030838
30. Mahalingam SM, Chu H, Liu X, Leamon CP, Low PS. Carbonic anhydrase IX-targeted near-infrared dye for fluorescence imaging of hypoxic tumors. *Bioconjugate Chem*. 2018;29(10):3320–3331. doi:10.1021/acs.bioconjchem.8b00509
31. Yang C, Xue Z, Liu Y, et al. Delivery of anticancer drug using pH-sensitive micelles from triblock copolymer MPEG-b-PBAE-b-PLA. *Mater Sci Eng C Mater Biol Appl*. 2018;84:254–262. doi:10.1016/j.msec.2017.12.003
32. Chen Q, Zheng J, Yuan X, Wang J, Zhang L. Folic acid grafted and tertiary amino based pH-responsive pentablock polymeric micelles for targeting anticancer drug delivery. *Mater Sci Eng C Mater Biol Appl*. 2018;82:1–9. doi:10.1016/j.msec.2017.08.026
33. Yang YT, Di Pasqua AJ, He W, et al. Preparation of alginate beads containing a prodrug of diethylenetriaminepentaacetic acid. *Carbohydr Polym*. 2013;92(2):1915–1920. doi:10.1016/j.carbpol.2012.11.071
34. Kamada H, Tsutsumi Y, Yoshioka Y, et al. Design of a pH-sensitive polymeric carrier for drug release and its application in cancer therapy. *Clin Cancer Res*. 2004;10(7):2545–2550. doi:10.1158/1078-0432.CCR-03-0544
35. Kang SI, Bae YH. pH-induced solubility transition of sulfonamide-based polymers. *J Control Release*. 2002;80(1–3):145–155. doi:10.1016/S0168-3659(02)00021-4
36. Cyphert EL, von Recum HA, Yamato M, Nakayama M. Surface sulfonamide modification of poly(N-isopropylacrylamide)-based block copolymer micelles to alter pH and temperature responsive properties for controlled intracellular uptake. *J Biomed Mater Res A*. 2018;106(6):1552–1560. doi:10.1002/jbm.a.36356
37. Xiao K, Li Y, Luo J, et al. The effect of surface charge on in vivo biodistribution of PEG-oligocholic acid based micellar nanoparticles. *Biomaterials*. 2011;32(13):3435–3446. doi:10.1016/j.biomaterials.2011.01.021
38. Shen X, Dirisala A, Toyoda M, et al. pH-responsive polyzwitterion covered nanocarriers for DNA delivery. *J Control Release*. 2023;360:928–939. doi:10.1016/j.jconrel.2023.07.038
39. Kim JH, Verwilst P, Won M, et al. A small molecule strategy for targeting cancer stem cells in hypoxic microenvironments and preventing tumorigenesis. *J Am Chem Soc*. 2021;143(35):14115–14124. doi:10.1021/jacs.1c03875
40. Mod Razif MRF, Chan SY, Widodo RT, et al. Optimization of a luteolin-loaded TPGS/Poloxamer 407 nanomicelle: the effects of copolymers, hydration temperature and duration, and freezing temperature on encapsulation efficiency, particle size, and solubility. *Cancers*. 2023;15(14):3741. doi:10.3390/cancers15143741